On Deploying Secondary Networks in Co-channel Bands with DTV Networks

Anshul Thakur and Swades De

***Abstract*—This paper explores the feasibility and scope of co-channel coexistence between a low data rate Orthogonal Frequency Division Multiplexing (OFDM) secondary network and a digital television (DTV) broadcast network operating in the same area. Since DTV receivers do not transmit, neither the presence nor the impact of interference from the secondary network on these DTV receivers can be known. Consequently, conventional spectrum sensing techniques cannot be employed effectively. This paper proposes to compensate the lack of feedback by combining the available information about population distribution in the region - ranging from coarse population density estimates to accurate geospatial maps - with better estimation of interference using a data-driven technique called Ordinary Kriging. Radio Environment Maps constructed using the Kriging method from field-reported observations from the secondary nodes are used to obtain better accuracy than the conventional statistical models. The estimates are then used to compute communication parameters for each secondary link in terms of power, number of active subcarriers, and active time slots, while keeping the average interference in the DTV network within threshold bounds. Thus, the viability of such co-channel license-exempt operation of secondary networks in the DTV black and grey spaces for low data rate applications in densely populated urban areas and higher data rate capabilities for sparsely populated rural areas is established.**

***Index Terms*—DTV band transmission, cognitive radio, Kriging, interference minimization**

I. Introduction

The number of wireless devices being added to the network has been rising at an unprecedented rate. Radio spectrum being a finite resource, this further strains the already burdened spectrum with increased interference, and consequently, decreased network performance. The spectrum scarcity problem has become one of the main research focuses. While higher frequencies are suited for short-range point-to-point communication, regulatory agencies worldwide have been focusing on the efficient reuse of the television (TV) bands for non-broadcasting purposes as well.

A. Motivation and contribution

Spectral underutilization in the traditional fixed spectrum allocation in the TV bands has been widely documented [1]. TV White Space (TVWS) technologies have tried to address this issue by performing trade-offs between achieving a high level of protection of the incumbent network, and a high amount of spectrum availability for network access by secondary systems [2] through a centralized database. These TVWS databases operate on the basis of network modeling and measurement campaign data, targeting coverage of the signal solely from the TV transmitters as a criterion for network presence.

However, these methods fall short in the face of changing dynamics of viewership as the techniques involved remain transmitter-centric and slow. While the households relying on Over-the-Air (OTA) broadcast services is already low [3], [4], this inefficiency is further exacerbated as the percentage of households using TV fluctuates from 7.6% during midnight to 60% during prime time [5]. Thus, even from the perspective of TV viewers, the active TV channels are spatially as well as temporally underutilized, which creates excess interference margins. Consequently, it is imperative to look into secondary spectrum access in legacy TV coverage areas where active TV receivers are present, also known as TV black-spaces (TVBS), and the areas without active TV receivers, also known as TV gray-spaces (TVGS). In particular, a large fraction of the devices being added to the ecosystem is being used for Internet of Things (IoT) monitoring applications, which have low data rate requirements. Leveraging the TVBS and TVGS for such IoT monitoring applications would help offload such traffic from the licensed bands.

Owing to the unidirectional nature of DTV broadcast, the biggest challenge of utilizing an active TV channel is to detect the presence of active DTV receivers, which act as hidden nodes. While some new standards, such as ATSC 3.0, are evolving to cater to an interactive TV experience requirement by making optional provisions for feedback via an OTA channel, it will take time before the technology gains widespread adoption. Meanwhile, techniques to work around the issue of hidden nodes need to be investigated with minimal or no changes in the existing DTV networks. As no direct method of feedback from the DTV receivers is available, the problem is broken into two steps: estimating the locations of active DTV receivers, and finding the signal conditions and interference impact at those DTV receivers.

For estimating the locations of the DTV receivers, the simplest way is to use the local population density estimates with an appropriate spatial distribution function. A more insightful method is to use geospatial maps tagged with positions of buildings along with TV ownership and viewership data. The population density estimate based method provides the baseline performance metric while the use of geospatial maps is explored in this work.

Having found the prospective locations of the DTV receivers, the signal conditions at those locations can be computed using statistical propagation models or data-driven mod-

A. Thakur is with Center for Development of Telematics, New Delhi, and the Department of Electrical Eng., IIT Delhi, New Delhi, India (e-mail: anshul.thakur@ee.iitd.ac.in). S. De is with the Department of Electrical Eng. and Bharti School of Telecommun., IIT Delhi, New Delhi, India (e-mail: swadesd@ee.iitd.ac.in).

els. As the coverage area of DTV networks is relatively large (with coverage radius often greater than 50 km), there is much variability of signal conditions and local spectrum availability within the coverage region, which cannot be captured in the statistical models [6]. This motivates the use of dynamic planning of radio resources for secondary access to manage the trade-off between interference from secondary users to the DTV receivers and to exploit the excess interference margin [7]. Data-driven Radio Environment Maps (REM) based on the Kriging method are known for good accuracy and low complexity, which can be used for improving overall spectral utilization [8]. The performance of the Kriging method is compared with the statistical method in this work.

The major contributions of this paper are as follows:

1) The feasibility of deploying low data rate secondary networks in co-channel mode within the coverage area of a DTV network without any feedback from the DTV network is explored.
2) Data-driven Kriging method of signal estimation is shown to improve the quality of estimates over statistical path loss models significantly. While deploying a low data rate secondary network with only statistical information of the DTV receiver density, the Kriging method outperforms the path loss model based method and keeps the DTV network outage within threshold by accounting for any local spatial correlation in signal conditions.
3) The combined use of geospatial tagged maps to derive DTV receiver information and the Kriging method for signal estimation is shown to provide secondary link coverage comparable to the case when exact information about the DTV receivers is available. Further, this allows the secondary network to dynamically adapt its transmission parameters according to the DTV receiver availability in the region.
4) The limited viability of employing temporal DTV viewership fluctuations through the day in dense population clusters is also shown through simulations.

B. Organization

The paper is organized as follows. In the next section, a survey of related works is presented. In Section III, the system model is presented, and expressions for the outage in the DTV network in an interference-limited scenario are obtained. The use of the Kriging method is described in Section IV. Performance results are presented and discussed in Section V. Finally, concluding remarks are drawn in Section VI.

II. Related Works

Several concerns need to be addressed while deploying a secondary network inside TVBS and TVGS. The concerns range from the feasibility of such deployment, to the interference impact on the TV receivers and how the geographically distributed access opportunity can be used by the secondary networks to improve performance.

Coexistence opportunity: Coexistence studies of DTV broadcast technologies like Digital Video Broadcast-Terrestrial second-generation (DVB-T2) with major Orthogonal Frequency Division Multiplexing (OFDM) based technologies such as Long Term Evolution (LTE) [9], IEEE 802.15.4m [10], and IEEE 802.22 WRAN [11] conducted in laboratory environments, and small-scale pilots indicate the feasibility of co-channel reuse. Opportunities arising from architectural differences between an OFDM-based DTV broadcast technology [12] and other bidirectional OFDM systems were systematically explored in [13], [14], and a framework for computing aggregate interference on the DTV receiver due to the secondary signal was proposed. The feasibility of deploying low data rate secondary nodes with low Signal to Noise and Interference Ratio (SINR) in TV Black spaces (TVBS) using interference cancellation was shown in [15].

Network-wide aggregate interference impact of secondary access points distributed in the primary network's coverage region using Poisson Point Process model was studied in [16], [17] while assuming a uniform signal transmission model. The same assumption cannot be made for networks deployed in the TV coverage areas due to fluctuating interference margin caused by large variability of the TV signal. Cooperative sensing has been used in [18], [19] to obtain the aggregate interference due to the secondary nodes, while channel access opportunity is cooperatively sensed in [20]. But these studies assume that the presence of the DTV receivers can be known through sensing which is not possible in the conventional DTV networks.

TV spectrum availability: Various studies have documented the underutilization of the TV bands using TV station registrations, radio propagation models and field surveys across the world [3], [6], [21]. However, it has been noted that the values chosen for various parameters such as shadow margin in the propagation models [22] used in these studies are usually too high, which reduces the spectrum usage efficiency [23]. Further, statistical models do not capture spatial variability in fade margins [24], and underestimate the availability of spectrum by ignoring the effects of various factors such as shadowing, penetration losses, etc. [25]. To this end, measurement-based enhancements, such as large spectrum sensing networks [26], and radio environment maps (REM) [18] have been proposed. While such approaches improve TVWS availability, they still suffer from spectral inefficiency due to the explicit focus on the primary transmitters while ignoring the primary receivers.

A static spectrum map created with the help of mandatory TV receiver registration data is used in [1] to refine spectrum availability in TVGS. However, such an approach is viable in small demographics only. The use of techniques such as beamforming, interference cancellation (IC), and TV receiver-assisted spectrum access to restrict the interference footprint of secondary networks have been demonstrated in the gray-spaces [3], [27]. Such approaches of utilizing information about DTV receivers is particularly useful in boosting spectral efficiency since a small fraction of the TV receivers are found to be active at any instant of time [5]. However, it implies significant upgrades at all the TV receiver locations to enable such feedback.

TV receiver sensing: The existing studies mostly use LBT to sense the presence of active TV receivers [28] before channel

access. However, the TV receivers pose a unique hidden terminal problem without any transmit capability, which cannot be solved through LBT. Diverse methods of sensing active TV receivers, such as detecting receiver's local oscillator's leakage power [29], voluntary TV registrations [1], attaching additional devices such as Neilsen meters or smart remotes [27] have been proposed. The approaches assume secondary nodes colocated with DTV receivers [30] or assume the existence of a cooperative agreement between the broadcaster and the secondary network operators, neither of which may be feasible. Adopting the next generation terrestrial TV standard (ATSC 3.0) offers another way of sensing the presence of TV receivers in the area in real-time by listening to the uplink channel [31]. Such feedback mechanisms already exist in various practical systems, such as channel quality indicator feedback in HSDPA, and ACK/NAK feedback in cellular or WiFi networks and has been widely studied [3], [6], [32]. However, it implies a massive overhaul of the existing DTV networks.

Various proposals also sought to solve this problem without involving TV receivers. This may be achieved through low power coexistence [33], or through the utilization of TV gray-spaces by measurement campaigns [1]. The notion of the existence of a critical DTV receiver, which, if protected, implies the protection of all other DTV receivers in the coverage area [12], [13]. In [12], a cooperative paradigm was considered where the secondary nodes have access to the DTV signal and bury their own precoded signal inside the DTV signal while amplifying the DTV signal acting like transmitters in the DTV Single Frequency Network. Other than location information of active DTV receivers, the accuracy of SINR estimates at the respective locations also limits the performance of the secondary system [34]. In order to estimate the SINR at various locations, the secondary network maintains some form of a dynamic Radio Environment Maps (REM) of the coverage area by sensing the primary signal [35].

Radio environment mapping: REM is a spatial and/or temporal profile of average signal powers in the area. The secondary network can then use this REM to evaluate its access opportunities and adapt the communication parameters to improve its performance as well as the efficiency of spectrum sharing [36]. REMs may be created using purely analytical path loss models, purely data-driven methods, or a combination of the two approaches. The creation of data-driven REMs often involves two major steps - localization and measurement of signal conditions at various sampling points, and interpolation of signal conditions across the entire coverage area. The localization step may employ Global Positioning System or methods based on Received Signal Strength Indication (RSSI) [37] such as simple trilateration [38], or Bayesian estimation [39], or a combination of these through crowd-sourced sensing [35]. The method used depends on various factors, such as terrain, indoor or outdoor environment, cost-effectiveness, and complexity [40]. Purely analytical path loss model based methods fail to account for the combined environmental effects of shadowing, penetration, and path loss at a granular level owing to the single environment assumption.

Conventional methods for interpolating the signals, such as Inverse Distance Weighted interpolation and Natural Neighbor interpolation [41], driven by data from sample points on the fields yield better performance due to improved spatial and temporal granularity. However, the errors in the localization step and interpolation step tend to get amplified, leading to a biased estimation with a wide error variance [34]. Instead, purely measurement-based methods of REM construction exist, such as the Kriging method, which model all the errors in a single step. The Kriging method, a form of Gaussian regression, optimizes the interpolation value by minimizing the error variance. Lately, it has been used by researchers in the wireless communication domain due to its high accuracy when compared to the existing analytical methods [34], [42]–[44], even with fewer sampling points. The change in signal values due to path loss creates an underlying trend. When considering interpolation over a small area, such a trend can usually be ignored without much loss of accuracy, and Ordinary Kriging method is used [45], [46]. However, when the trend is significant, then the application of Ordinary Kriging is preceded by elimination of the trend from the samples using various techniques such as Ordinary Least Squares [47], Residual Maximum Likelihood Estimation [8], [48], and Neural Networks [47]. Further, the error in its interpolated received powers can be modeled using a correlation coefficient for analytical tractability as well [49].

It is intuitive that the information about the signal conditions at active TV receivers benefits the secondary networks and increases the overall spectral efficiency. While the feasibility of co-channel coexistence for low data rate communication has been demonstrated, the existing studies have relied mainly on the assumption that either channel sensing can detect the incumbent users or that some form of feedback is available. Indirect means of obtaining active DTV receiver locations, such as user registrations or ground surveys, have scale limitations and are highly static. Moreover, the use of statistical path loss models limits the accuracy in the case of large coverage regions of the DTV networks, and consequently, the performance of the secondary networks.

Since DTV receivers are expected to be mainly located in households, this work explores the use of geospatial maps and TV ownership statistics to estimate the locations of DTV receivers. To overcome the limitations of statistical path loss models, a data-driven Kriging method is used to construct accurate REMs from the observed signal conditions at the secondary nodes' locations to improve the accuracy of signal estimates at the locations of DTV receivers. The system model used for evaluating the impact of interference and the performance of the coexisting systems in terms of outage probability is presented in the next section.

III. System Model

Let us consider the deployment topology illustrated in Fig. 1. A DTV broadcast transmitter $\mathrm{Tx}^{(\mathrm{D})}$ positioned at coordinate $\mathbf{x}_t^{(D)}$ serves the DTV receivers in the region $\mathbb{A}$, $\mathbb{A} \in \mathbb{R}^2$ over a single channel by transmitting an OFDM signal with useful symbol duration $T_u^{(D)}$ over $N^{(D)}$ subcarriers.

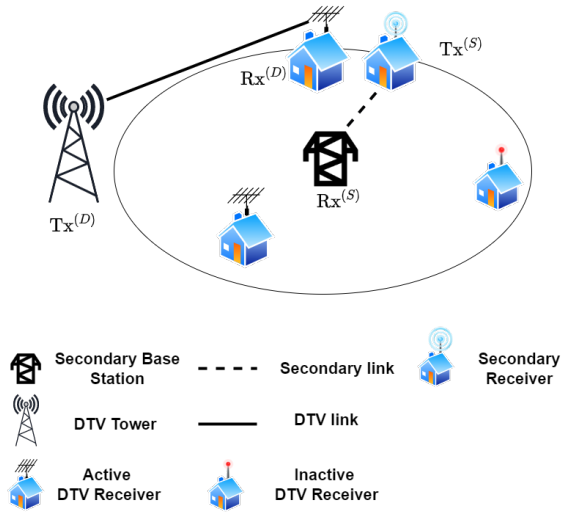

Fig. 1. Network topology for secondary network operation in the DTV band in co-channel mode within protection contour.

An LTE-like OFDM-based secondary communication network operates its uplink in co-channel mode with the DTV band within a small subset region c of the coverage area $\mathbb{A}$. Downlink communication is not considered in this co-channel scheme as it is assumed to be sporadic, largely used for instructing the secondary IoT nodes to send data. The secondary network consists of a Base Station (BS) $\text{Rx}^{(S)}$ positioned at $\mathbf{x}_r^{(S)}$ which services M nodes located at $\{\mathbf{x}_i^{(S)}\}_{i=1}^{M}, \forall \mathbf{x}_i^{(S)} \in c$ distributed according to a 2-dimensional homogeneous Poisson process with intensity $\lambda^{(S)}$. The secondary node farthest from the BS is of particular interest and hence, is marked individually as $\text{Tx}^{(S)}$ at its coordinate $\mathbf{x}_t^{(S)}$. The secondary network employs a total symbol duration of $T^{(S)}$, ($T^{(S)} \ll T_u^{(D)}$) with a variable number of subcarriers subject to a maximum of $N^{(S)}$. The secondary uplink operation is time aligned with the DTV symbols such that a maximum of L contiguous secondary OFDM symbols slots can be received during a single DTV symbol, i.e. $L = \left\lfloor T_u^{(D)}/T^{(S)} \right\rfloor$.

The secondary network is capable of varying the number of time slots and occupied subcarriers along with adaptive power control to keep interference within acceptable bounds. Further, the nodes are capable of decoding the DTV signal and, consequently, performing (perfect) interference cancellation. All the secondary nodes report the measured DTV signal power at their respective locations to the BS $\text{Rx}^{(S)}$. The BS computes the transmission parameters to be used by each secondary node in its uplink by accounting for the interference constraints and communicates the parameters to the respective nodes in the downlink channel. The secondary network must maintain an SINR of $\Gamma_{th}^{(S)}$ with an outage probability of $p_{out,th}^{(S)}$ for the considered modulation scheme.

Unknown to the secondary nodes, there are U hidden, active DTV receivers distributed in the secondary coverage region c at coordinates $\{\mathbf{x}_i^{(D)}\}_{i=1}^{U}, \forall \mathbf{x}_i^{(D)} \in c$. For the chosen operating parameters of the DTV network, a threshold SINR of $\Gamma_{th}^{(D)}$ must be maintained with an outage probability of $p_{out,th}^{(D)}$ for an error-free viewing experience. The method used at the BS to compute the SINR condition estimates at the victim DTV receivers depends on the amount of data available, as will be explained further.

The environment is assumed to exhibit log-normal shadowing with a shadowing coefficient of σ_D for the DTV transmission and a path loss factor of η. This coefficient does not change during the period of observation. Perfect channel information from the secondary nodes $\{x_i^{(S)}\}_{i=1}^{M}$ is assumed available at the BS $\text{Rx}^{(S)}$. The power terms considered subsequently are in their logarithmic form unless specified otherwise. The use of average powers levels overcomes the effects of fading on the signal. A glossary of all symbols used in this paper is listed in Table I.

IV. Interference Analysis

In the absence of any direct feedback from the DTV receivers active in the region, the secondary nodes need to be able to estimate the interference impact via indirect methods. This estimation can be broken into two major sub-problems: locating the active DTV receivers, and estimating the signal conditions experienced at the respective location. This section discusses the methods used to solve these problems.

A. Critical DTV receiver and active DTV receivers distribution

Since precise information about the SINR experienced at the active DTV receivers in the coverage area c is not available with the BS, the BS employs different blind methods to estimate this SINR information.

Assuming that the coverage area of the secondary network is small, the DTV signal conditions in the vicinity of a secondary transmitter are assumed to be uniform. Then, the DTV receiver worst affected from the transmissions from a secondary transmitter $\text{Tx}^{(S)}$ positioned at $\mathbf{x}_t^{(S)}$ is the one closest to it. Further, if this critical DTV receiver is protected, any DTV receiver at a distance farther can be considered to be safely protected [12]. Let this critical DTV receiver $\text{Rx}^{(D)}$ be positioned at $\mathbf{x}_r^{(D)}$ at a distance $d_c = \left\| \mathbf{x}_t^{(S)} - \mathbf{x}_r^{(D)} \right\|$.

The distribution of active DTV receivers in the coverage area c as well as the distance of this hypothetical critical receiver from the secondary transmitter may be estimated according to the various degrees of information available. The simplest method is to use easily available statistical estimates such as the household density in the area. More information on households can be gathered from geospatial maps by tagging the households and accounting for the possibility of an active DTV receiver in the household. Apart from the household density, the Over-the-air (OTA) TV ownership rate influences DTV viewership. It has been observed that urban areas exhibit a very low OTA TV ownership rate $O(c)$ [3], despite high household density. Further, time of the day and ratings of programs airing during the duration greatly influences the viewership statistic [50] and can be taken into account when not computing secondary parameters for the worst case. By the law of large numbers, the probability $p_{act}(t)$ of a DTV receiver being active at a time is equal to the cumulative ratings of all

TABLE I
GLOSSARY OF SYMBOLS USED

Notation	Description
$\mathbb{A}$	Total DTV coverage area
c	Secondary coverage area inside $\mathbb{A}$
M	Number of secondary nodes in the region c
U	Number of active DTV receiver nodes in the region c
$\lambda^{(S)}$	Secondary node distribution density in region c
$\lambda^{(D)}$	Active DTV receivers distribution density in region c
$O(c)$	OTA TV Ownership rate in area c
$p_{act}(t)$	Cumulative channel rating at time t
$\text{Tx}^{(\text{D})}$	DTV Transmitter
$\text{Rx}^{(D)}$	DTV receiver
$\text{Rx}^{(S)}$	Secondary uplink receiver BS
$\text{Tx}^{(S)}$	Secondary uplink transmitter
$T_u^{(D)}$	Useful symbol duration of DTV signal
$T_u^{(S)}$	Useful symbol duration of secondary signal
$T^{(S)}$	Total symbol duration of secondary signal
$\Delta f^{(S)}$	Frequency offset between DTV and secondary signals
$N^{(D)}$	Total subcarriers in DTV signal
$N^{(S)}$	Active subcarriers in secondary signal
$\mathbf{x}_i^{(S)}$	Coordinates of secondary nodes
$\mathbf{x}_j^{(D)}$	Coordinates of DTV nodes
d_c	Distance of a secondary node from its critical DTV receiver
d_{cor}	Decorrelation distance of the shadowing process
d_i	Distance of ith secondary node from DTV transmitter
L	Number of symbol slots occupied by secondary in $T^{(D)}$
$\Gamma^{(D)}$	Average SINR experienced at the DTV receiver
$\Gamma_{th}^{(D)}$	Threshold SINR required at the DTV receiver
$\Gamma_{th}^{(S)}$	Threshold SINR required at the secondary receiver
χ	Average DTV power to interference power ratio experienced at the DTV receiver
χ_{th}	Threshold DTV power to interference power ratio experienced at the DTV receiver
$p_{out}^{(D)}$	Outage probability in the DTV network
$p_{out,th}^{(D)}$	Threshold outage probability in the DTV network
$p_{out}^{(S)}$	Outage probability in the secondary link
$p_{out,th}^{(S)}$	Threshold outage probability in the secondary link
$P_t^{(D)}$	Power transmitted by the DTV transmitter
$P_t^{(S)}$	Power transmitted by the secondary transmitter
$P_r^{(D)}$	DTV signal power received by the DTV receiver
$\hat{P}_r^{(D)}$	Estimated DTV signal power received by the DTV receiver
$P_r^{(S)}$	Secondary signal power received by the DTV receiver
η	Path loss exponent for DTV signal
σ_D	Shadowing coefficient for the DTV signal
$\Psi^{(D)}$	Log-Normal shadowing process for the DTV signal
$H_l^{(D)}$	Channel gain on the lth DTV subcarrier
I_l	Interference gain on the lth DTV subcarrier due to secondary co-channel transmission
$H^{(D)}$	Channel gain in the DTV signal
$I^{(S)}$	Interference gain caused at the DTV receiver due to secondary node transmission
γ	Analytical semivariogram of DTV signals sampled spatially
$\hat{\gamma}$	Empirical semivariogram of DTV signals sampled spatially

TV programs being broadcast in that band during the duration [3].

Thus, when only coarse statistical estimates such as household density and OTA TV ownership rates are available, a Poisson distribution [16] of DTV receivers with density $\lambda^{(D)}$ is assumed. $\lambda^{(D)}$ can be taken as the product of household density and OTA TV ownership rate $O(c)$ in the area c. Since the location of the DTV receivers is purely driven by an underlying distribution rather than ground data, channel ratings are not used in this model. The mean distance d_c of the nearest DTV receiver from any sampled point can be computed analytically.

When positions of all households is available via geospatial maps, the probability of having an active DTV receiver at each position is simply $O(c)p_{act}$. Distance d_c of the critical DTV receiver from the secondary transmitter can be known from the geospatial map. Further, when all the prospective DTV receivers in the coverage region can be mapped, the notion of just the critical receiver can be eschewed in favor of protecting all the DTV receivers for more robust estimates.

B. Signal conditions estimation at DTV receiver locations

Once the prospective locations of DTV receivers are known, the prevailing DTV signal conditions at the respective locations need to be estimated. Analytical path loss and shadowing models can be used to provide low complexity estimates. These models have the advantage that no further information from the secondary nodes distributed in the coverage area is required to compute the operating parameters. The true power $P_r^{(D)}(\mathbf{x})$ received at the DTV receiver at position $\mathbf{x}$ can be expressed as

$$\begin{aligned} P_r^{(D)}(\mathbf{x}) &= P_t^{(D)} - K_c - 10\eta \log\left\|\mathbf{x}_t^{(D)} - \mathbf{x}\right\| + \Psi^{(D)}(\mathbf{x}) \\ &= P_c^{(D)} - 10\eta \log\left\|\mathbf{x}_t^{(D)} - \mathbf{x}\right\| + \Psi^{(D)}(\mathbf{x}) \\ &= \bar{P}(\mathbf{x}) + \Psi^{(D)}(\mathbf{x}) \end{aligned} \tag{1}$$

where K_c is the frequency dependent path loss factor, η is the path loss coefficient, and $\Psi^{(D)} \sim \mathcal{N}(0, \sigma_D^2)$ is the log-normal shadowing process . $P_c^{(D)}$ collects the frequency-dependent losses with the transmit power. Shadowing is assumed to be correlated spatially with a decorrelation distance with correlation d_{cor} for location pairs $(\mathbf{x}_i, \mathbf{x}_j)$ defined as

$$H_{i,j} = \exp \frac{-\left\|\mathbf{x}_i - \mathbf{x}_j\right\| \ln 2}{d_{cor}} \tag{2}$$

where d_{cor} is the spatial decorrelation distance defined as the distance satisfying $H_{i,j} = 0.50$. Small-scale fading is assumed to be eliminated owing to long-term measurements. Further, an interference dominant scenario is considered, hence, additive white Gaussian noise (AWGN) is assumed to be negligible. For notional consistency, the term SINR is used throughout this work even though the noise component is not considered significant when considering the interference dominated scenario.

The statistical models fail to accurately capture topographic variations that result in irregular and correlated shadowing across various closely spaced locations. Ordinary Kriging interpolation creates better estimates as it takes into account

the second-order properties of the underlying process that has an unknown mean and variance. All the M secondary nodes measure the signal power received at their respective locations due to the DTV transmitter $\text{Tx}^{(\text{D})}$ and communicate to the BS. The collected power measurements at the BS are maintained as a vector $\mathbf{y} \sim \mathcal{N}(\mathbf{X}\boldsymbol{\beta}, \mathbf{C}(\boldsymbol{\theta}))$. $\mathbf{X}$ and $\boldsymbol{\beta}$ are defined as

$$\mathbf{X} = \begin{pmatrix} 1 & -10\log(d_1) \\ 1 & -10\log(d_2) \\ \vdots & \\ 1 & -10\log(d_M) \end{pmatrix}, \quad \boldsymbol{\beta} = \begin{pmatrix} P_c^{(D)} \\ \eta \end{pmatrix} \tag{3}$$

where $d_i = \left\| \mathbf{x}_i^{(S)} - \mathbf{x}_t^{(D)} \right\|$. $\mathbf{C}(\boldsymbol{\theta})$ is the variance-covariance matrix defined in terms of parameters termed as nugget, sill, and range, as $\mathbf{C}(\boldsymbol{\theta}) = p_1\mathbf{I} + p_2\mathbf{H}(p_3)$. For Kriging methods, $\mathbf{C}(\boldsymbol{\theta})$ is the semivariogram model chosen where, $\boldsymbol{\theta}$ is the parameter vector consisting of these parameters, $\mathbf{I}$ is an $M \times M$ identity matrix, $\mathbf{H}(p_3)$ is an $M \times M$ matrix.

The goal is to estimate the unknown value $\hat{P}_r^{(D)}(\mathbf{x})$ at an arbitrary location $\mathbf{x}$, where the DTV receiver $\text{Rx}^{(\text{D})}$ is located by using a weighted sum of all the measurement points from the M nodes as

$$\hat{P}_r^{(D)}(\mathbf{x}) = \sum_{i=1}^{M} \omega_i P_r^{(D)}(\mathbf{x}_i) \tag{4}$$

where $\omega_i (i = 1, \ldots, M)$ are the weights assigned to the data points such that the variance σ_k^2 of estimation error ϵ is minimized, $\hat{\eta}$ is the estimated path loss coefficient, $\hat{P}_c^{(D)}$ is the estimated $P_c^{(D)}$, $\hat{P}_r^{(D)}(\mathbf{x})$ is the interpolated value; the true value being $P(\mathbf{x})$. The error ϵ at $\mathbf{x}$ is expressed as $\epsilon(\mathbf{x}) = P_r^{(D)}(\mathbf{x}) - \hat{P}_r^{(D)}(\mathbf{x})$. The weights obtained take into account the spatial correlation between the samples. For the best linear unbiased estimator, the following constraint is set

$$\sum_{i=1}^{M} \omega_i = 1. \tag{5}$$

To use Kriging, an estimate of the spatial covariance, path loss coefficient, and frequency-dependent losses is usually required prior to the interpolation process. In the relatively small coverage areas of the secondary network, the path loss in the DTV signal tends to be slow, and the mean value can be considered almost constant for the considered distances [12]. Under this constant (unknown) mean assumption, Ordinary Kriging offers the best trade-off between complexity and performance among various Kriging methods. Further, Ordinary Kriging does not involve an explicit estimation of the parameters in $\boldsymbol{\beta}$. A data-driven empirical estimate $\bar{\gamma}(\mathbf{x_i}, \mathbf{x_0})$ of the spatial-covariance structure of the random process known as the semi-variogram $\gamma(\mathbf{x_i}, \mathbf{x_0})$ is obtained using the dataset. The empirical semi-variogram $\gamma(\mathbf{d})$ used in Ordinary Kriging is the semivariance of the difference of all pairs of points, $P_r^{(D)}(\mathbf{x}_i)$ and $P_r^{(D)}(\mathbf{x}_j)$, at distance h. Under the constant mean power assumption, the unbiased estimator can be expressed as

$$\begin{aligned} \hat{\gamma}(\mathbf{d}) &= \frac{1}{2|N(\mathbf{d})|} \sum_{N(\mathbf{d})} Var(P_r^{(D)}(\mathbf{x}_i) - P_r^{(D)}(\mathbf{x}_j)) \\ &= \frac{1}{2|N(\mathbf{d})|} \sum_{N(\mathbf{d})} (P_r^{(D)}(\mathbf{x}_i) - P_r^{(D)}(\mathbf{x}_j))^2, \ \mathbf{d} \in \mathbb{R}^2 \end{aligned} \tag{6}$$

where $N(\mathbf{d})$ denotes the set of nodes (i, j) separated by a distance $d = \left\| \mathbf{x}_i - \mathbf{x}_j \right\|$. Once the $\hat{\gamma}(.)$ is estimated, it is fitted into one of the several models available in literature to allow the use of the semivariogram across unsampled locations as well [51]. The usual methods employed to fit the semi-variogram are derived from least squares estimation. Two isotropic models that are frequently employed for REM construction while considering correlated shadowing are - the Gaussian model:

$$\bar{\gamma}(\mathbf{d}) = p_1 + p_2 \left(1 - \exp\left(\frac{-\mathbf{d}}{p_3} \right)^2 \right) \tag{7}$$

and the exponential model:

$$\bar{\gamma}(\mathbf{d}) = p_1 + p_2 \left(1 - \exp\left(\frac{-\mathbf{d}}{p_3} \right) \right). \tag{8}$$

As will be seen later, the exponential semivariogram performs better than the Gaussian semivariogram.

With $\mathcal{L}(\mathbf{x}_0)$ as the Lagrange multiplier, the objective function for minimization under the constant mean assumption at location $\mathbf{x}_0$ can be expressed as

$$\begin{aligned} &\mathbb{E}\left[(P(\mathbf{x}_0) - \hat{P}(\mathbf{x}_0))^2 \right] - 2\mathcal{L}(\mathbf{x}_0)(\sum_{i=1}^{M} \omega_i - 1) \\ &= \mathbb{E}\left[(P(\mathbf{x}_0) - \sum_{i=1}^{M} \omega_i P_r^{(D)}(\mathbf{x}_i))^2 \right] - 2\mathcal{L}(\mathbf{x}_0)(\sum_{i=1}^{M} \omega_i - 1) \\ &= \mathbb{E}\left[-\sum_{i=1}^{M}\sum_{j=1}^{M} \omega_i\omega_j \frac{(P(\mathbf{x}_i) - P(\mathbf{x}_j))^2}{2} + \right. \\ &\qquad \left. 2\sum_{i=1}^{M} \omega_i \frac{(P(\mathbf{x}_0) - P(\mathbf{x}_j))^2}{2} \right] - 2\mathcal{L}(\mathbf{x}_0)(\sum_{i=1}^{M} \omega_i - 1) \\ &= -\sum_{i=1}^{M}\sum_{j=1}^{M} \omega_i\omega_j\gamma(\mathbf{x}_i - \mathbf{x}_j) + \\ &\qquad 2\sum_{i=1}^{M} \omega_i\gamma(\mathbf{x}_0 - \mathbf{x}_i) - 2\mathcal{L}(\mathbf{x}_0)(\sum_{i=1}^{M} \omega_i - 1). \end{aligned} \tag{9}$$

On differentiating (9) with respect to ω_i $i \in (1, \ldots, M)$ and $\mathcal{L}(\mathbf{x}_0)$ and equating the expression to 0, the optimal values of ω_i that minimize the variance σ_k^2 satisfy

$$\sum_{i=1}^{M} w_i(\mathbf{x})\gamma(\mathbf{x_i}, \mathbf{x_j}) + \mathcal{L}(\mathbf{x}) = \gamma(\mathbf{x_i}, \mathbf{x_0}), \qquad i = 1, \ldots, M. \tag{10}$$

The expression in (4) can be expanded in terms of the signal

propagation model of (1) as

$$\hat{P}_r^{(D)}(\mathbf{x}) = \hat{P}_c^{(D)} - 10\hat{\eta}\log\left\|\mathbf{x}_t^{(D)} - \mathbf{x}\right\| + \sum_{i=1}^{M}\omega_i\left(P_r^{(D)}(\mathbf{x}_i) - \left(\hat{P_c^{(D)}} - 10\hat{\eta}\log\left\|\mathbf{x}_t^{(D)} - \mathbf{x}_i\right\|\right)\right) \tag{11}$$

where $\hat{P}_c^{(D)} - 10\hat{\eta}\log\left\|\mathbf{x}_t^{(D)} - \mathbf{x}\right\|$ is the effective path loss term at location $\mathbf{x}$ and is treated as the unknown mean in the small area under consideration. Since the received power follows log-normal distribution and its estimated value is correlated, $\left(P_r^{(D)}(\mathbf{x}), \hat{P}_r^{(D)}(\mathbf{x})\right)$, and consequently $\epsilon(\mathbf{x})$ follows a bivariate normal distribution [49] with a mean value of $\bar{P}(\mathbf{x})$ and a variance-covariance matrix expressed as

$$\begin{pmatrix} \sigma_D^2 & \rho\sigma_D\hat{\sigma}_D \\ \rho\hat{\sigma}_D\sigma_D & \hat{\sigma}_D^2 \end{pmatrix} \tag{12}$$

where ρ is the correlation coefficient between $P_r^{(D)}((x))$ and $\hat{P}_r^{(D)}((x))$. The variance of error is then given as

$$\sigma_k^2 = \sigma^2 + \sigma_{\hat{p}}^2 - 2\rho\sigma\sigma_{\hat{p}}. \tag{13}$$

The error variance is minimized when $\hat{\sigma}_D = \rho\sigma_D$. Since Kriging minimizes the error variance under the constraints in (5), the error variance can be approximated as $\sigma_k^2 = \sigma_D^2(1-\rho^2)$. Thus, the correlation factor can be used directly in the estimated path loss models to account for Kriging's model accuracy. For a DTV receiver at position $\mathbf{x}$, the estimated power $\hat{P}_r^{(D)}(\mathbf{x})$ expressed in (11) can be equivalently expressed as

$$\hat{P}_r^{(D)}(\mathbf{x}) = \hat{P}_c^{(D)} - 10\hat{\eta}\log\left\|\mathbf{x}_t^{(D)} - \mathbf{x}\right\| + \hat{\Psi}^{(D)}(\mathbf{x}) \tag{14}$$

where $\hat{\Psi}^{(D)} \sim \mathcal{N}(0, \hat{\sigma}_D(\rho)^2)$ is the estimated log-normal shadowing process with its variance, now a function of correlation ρ. It may be observed that, for a conventional shadowing model the correlation value may be set to 0, which reduces (14) to a form similar to (1). Though the estimation of actual ρ would still require the computation of σ_k^2, computational effort of large simulations while comparing and evaluating the performance of Kriging based signal estimation can be avoided by appropriately setting the values of ρ.

C. Interference at the DTV receiver

Interference at DTV receiver $\mathrm{Rx}^{(D)}$ located at $\mathbf{x}_c^{(D)}$ due to transmission from the secondary transmitter $\mathrm{Tx}^{(S)}$ depends on the operating parameters of the DTV network as well as the secondary network. For a seamless viewing experience, it is required that the average SINR $\Gamma^{(D)}$ at the DTV receiver does not reduce below a threshold $\Gamma_{th}^{(D)}$.

With uniform power allocation across all subcarriers, the SINR $\Gamma^{(D)}(\mathbf{x}_c^{(D)})$ at the DTV receiver $\mathrm{Rx}^{(\mathrm{D})}$ can be expressed in terms of the average signal power from broadcast transmitter $P_r^{(D)}(\mathbf{x}_c^{(D)})$, average interference power from the secondary transmitter $P_r^{(S)}(\mathbf{x}_c^{(D)})$, and the noise power at the DTV receiver N_o (all considered in their fractional form rather than logarithmic form)

$$\Gamma^{(D)}(\mathbf{x}_c^{(D)}) = \frac{P_r^{(D)}(\mathbf{x}_c^{(D)})E[\mid H^{(D)}\mid^2]}{P_r^{(S)}(\mathbf{x}_c^{(D)})E[\mid I^{(S)}\mid^2] + N_o}. \tag{15}$$

The aggregate average interference power gain $E[\mid I^{(S)}\mid^2]$ is the average of interference powers across all the OFDM subcarriers. In a heterogeneous OFDM system, the impact of interference on each subcarrier is computed as a weighted sum of interference powers of all the secondary OFDM subcarriers at the respective primary subcarrier. Interference on a subcarrier is expressed as [13]

$$\mathbb{E}[\mid I_l\mid^2] = \frac{1}{T_u^{(S)}T_u^{(D)}}\sum_{k=0}^{N^{(S)}-1}\left|H_k^{(S)}\right|^2 \times\left\{\sum_{b=0}^{L-1}\frac{\sin^2(\pi c(k)T^{(S)})}{\pi^2c^2(k)} + \frac{1}{\pi^2c^2(k)}\frac{T_1+T_2}{T^{(S)}}\right\} \tag{16}$$

where $\mid H_k^{(S)}\mid$ is the channel gain at the kth secondary subcarrier, and $c(k) = \Delta f^{(S)} + \frac{k}{T_u^{(S)}} - \frac{l}{T_u^{(D)}}$. T_1 and T_2 are obtained as

$$T_1 = \frac{T^{(S)}}{2} - \frac{\sin(2\pi c(k)(T_u^{(S)}))}{4\pi c(k)} + \frac{\sin(2\pi c(k)(-T^{(S)}+T_u^{(S)}))}{4\pi c(k)} \tag{17}$$

$$T_2 = \frac{T^{(S)}}{2} - \frac{\sin(2\pi c(k)((\xi'-L-1)T^{(S)}+T_u^{(S)}))}{4\pi c(k)} + \frac{\sin(2\pi c(k)((\xi'-L-2)T^{(S)}+T_u^{(S)}))}{4\pi c(k)} \tag{18}$$

An outline of the steps to derive the expression in (16) is provided in the appendix.

In an interference-limited scenario, if $\Gamma_{th}^{(D)}$ is the threshold SINR to be maintained at the active DTV receiver, then, the power-ratio χ_{th} that achieves this SINR is expressed as

$$\chi_{th} = P_r^{(D)} - P_r^{(S)} = 10\log_{10}(\Gamma_{th}^{(D)}E[\mid I^{(S)}\mid^2]). \tag{19}$$

D. Outage analysis

It is clear that the degree of availability of DTV receiver information determines the performance of the secondary network. For a viable deployment, the outage requirement in the DTV network must be met. Three cases are discussed while considering the outage performance:

1) Minimum information: Only statistical estimates of active DTV receiver locations are known
2) Positional information: All prospective DTV receiver locations are mapped, but active DTV receivers are not known
3) Benchmark: Complete information of active DTV receivers' signal conditions are known

Let χ be the average power-ratio at the critical DTV receiver $\mathrm{Rx}^{(\mathrm{D})}$ located at a distance $d_c = \left\|\mathbf{x}_c - \mathbf{x}_t^{(S)}\right\|$ from $\mathrm{Tx}^{(S)}$.

Since $P_r^{(D)}$ and $P_r^{(S)}$ are normally distributed (in logarithmic form), χ is also normally distributed as $\mathcal{N}(\mu_\psi, \sigma_\psi)$ with $\mu_\psi = P_r^{(D)} - P_r^{(S)}$ and $\sigma_\psi^2 = \sigma_D^2(\rho) + \sigma_s^2$ where ρ is the correlation factor between the estimated DTV signal power at the DTV receiver and its true value, which depends on the method used for interpolation. Then, conditional outage probability can be written as

$$P\{\chi \leq \chi_{th} | r = d_c\} = 1 - Q\left(\frac{\chi_{th} - (\mu_\psi)}{\sigma_\psi}\right) \tag{20}$$

where r is the distance between $\text{Tx}^{(S)}$ and $\text{Rx}^{(\text{D})}$.

When the possible locations of each DTV receiver is known through the use of demographic maps, the coordinate of the critical DTV receiver is known and (20) is used directly. However, when only statistical estimates for population density are used, the DTV receivers may be assumed distributed according to a two dimensional circular and homogeneous Poisson process with intensity $\lambda^{(D)}$ in the coverage radius r_c of the secondary network. The probability that an active DTV receiver is present at a distance r from $\text{Tx}^{(S)}$ can be calculated from the distribution function as $P(r = x) = 2\pi\lambda x e^{-\lambda\pi x^2}, \forall (x \geq 0)$. Thus, the expected outage $p_{out}^{(D)}$ can then be expressed as

$$\begin{aligned} p_{out}^{(D)} &= \mathbb{E}[P(\chi \leq \chi_{th}, r)] \\ &= \int_0^{r_c} P(\chi \leq \chi_{th}) P(r = d) dr \\ &= \int_0^{r_c} P(\chi \leq \chi_{th}) 2\pi\lambda r e^{-\lambda\pi r^2} dr \\ &= \int_0^{r_c} \left(1 - Q\left(\frac{\chi_{th} - \mu_\Psi}{\sigma_\Psi}\right)\right) .2\pi\lambda r e^{-\lambda\pi r^2} dr. \end{aligned} \tag{21}$$

Substituting (14) and (20) in (22) yields the average power $P_r^{(S)}$ received from $\text{Tx}^{(S)}$ in order to maintain the outage below $p_{out,th}^{(D)}$ as

$$P_r^{(S)} = P_r^{(D)} - \chi_{th} + \sigma_\psi Q^{-1}(1 - p_{out,th}^{(D)}). \tag{22}$$

The outage across the entire SU coverage area can then be easily computed based on the level of information available. When no demographic information is available, the coverage C where outage requirement $p_{out,th}^{(D)}$ is met over a coverage radius r_c is expressed as

$$\begin{aligned} C &= 1 - p_{out,th}^{(D)} \\ &= \frac{2}{r_c^2} \int_0^{r_c} rQ\left(a - b \ln\left(\frac{r}{d_p}\right)\right) dr \end{aligned} \tag{23}$$

where

$$\begin{aligned} a &= \frac{\chi_{th} - (P_t^{(D)} - P_t^{(S)})}{\sigma_{SINR}(\rho)} \\ b &= \frac{10\eta \log_{10} e}{\sigma_{SINR}(\rho)}. \end{aligned}$$

When the possible locations of each DTV receiver is known through the use of demographic maps, the outage at each DTV receiver must be considered. Then, for U active DTV receivers located at coordinates $\{\mathbf{x}_i^{(D)}\}_{i=1}^U, \forall \mathbf{x}_i^{(D)} \in c$,

$$\begin{aligned} p_{out}^{(D)} &= \frac{1}{U} \sum_{\mathbf{x}^{(D)_q}} \mathcal{I}_{\{P\{\chi^q < \chi_{th}, \mathbf{x}^{(D)_q}\}\}} \\ &= \frac{1}{U} \sum_{\mathbf{x}_\mathbf{q}^{(\mathbf{D})}} \mathcal{I}_{\{P\{\rho^q < \rho_{th} | \mathbf{x}_q^{(D)}\} P\{\mathbf{x}_q^{(D)}\}\}}. \end{aligned} \tag{24}$$

$P\{\mathbf{x}_q^{(D)}\}$ is the probability that an active DTV receiver is present at $\mathbf{x}^q$ and is expressed as

$$P\{\mathbf{x}_q^{(D)}\} = O(c) p_{act} \tag{25}$$

where $O(c)$ is the OTA ownership rate, and p_{act} is the cumulative rating of all the TV channels multiplexed on the current band. Numerically solving this problem for an outage constraint yields $P_{s,max}$ and r_c for the worst case.

TABLE II
POWER RATIOS REQUIRED TO MAINTAIN $\Gamma_{th}^{(dtv)}$ AT A DTV RECEIVER WITH A SECONDARY NETWORK. CENTER FREQUENCY $f_c^{(s)} = f_c^{(dtv)}$, $T_u^{(s)} = 66.7\ \mu s$

BW (kHz) \ Time slots	1	2	3	4	5	6
15	−22.34	−19.90	−18.35	−17.21	−16.31	−15.94
30	−18.15	−15.72	−14.17	−13.03	−12.12	−11.86
45	−16.00	−13.58	−12.03	−10.89	−9.99	−9.75
60	−14.56	−12.14	−10.59	−9.46	−8.55	−8.33
75	−13.48	−11.06	−9.51	−8.38	−7.47	−7.22
90	−12.61	−10.19	−8.65	−7.51	−6.61	−6.39
105	−11.88	−9.47	−7.931	−6.79	−5.89	−5.67
120	−11.26	−8.84	−7.30	−6.17	−5.27	−5.05
135	−10.71	−8.30	−6.76	−5.62	−4.73	−4.51
150	−10.23	−7.82	−6.28	−5.14	−4.24	−4.03
165	−9.79	−7.38	−5.84	−4.71	−3.81	−3.59
180	−9.40	−6.99	−5.45	−4.31	−3.41	−3.20

V. SIMULATION RESULTS AND DISCUSSION

This section discusses the simulation results and performance of the coexisting secondary network and the DTV network using the analysis presented above. A DTV network with parameters from Table III is simulated in a circular region of radius 50 km. When the tagged geospatial map is not available, the DTV receivers are placed according to a homogeneous 2-dimensional Poisson process. DTV receiver densities of 200 km^{-2} and 400 km^{-2} are used to represent typical rural, and urban cluster deployment densities [52]. OTA TV ownership rates, as well as TV viewership statistics [3], are taken into consideration for selecting the active DTV receivers. A secondary BS operating with parameters from Table IV is placed randomly in this coverage area with a similar deployment density and incorporates the outage calculations for managing the uplink communication. Table II captures the received threshold power ratios χ_{th} of the various combinations of active sub-carriers and occupied time slots in the secondary system that maintains the threshold SINR $\Gamma_{th}^{(D)}$

TABLE III
DTV (DVB-T2) TRANSMISSION PARAMETERS

Center frequency	429 MHz
Bandwidth	7.6094 MHz (8 MHz)
FFT size	4096
Active subcarriers	3409
Guard interval fraction	$1/32$
Code rate	$2/3$
Modulation	64 QAM
Symbol duration	448 μs
Threshold SINR	14 dB

TABLE IV
SECONDARY TRANSMITTER PARAMETERS

Bandwidth	180 kHz
Active Subcarriers	12
Modulation	QPSK
Symbol Duration	66.67 μs
Threshold SINR	-11.8 dB
Sensitivity	-141 dBm

at the DTV receivers. The outage probability for the DTV network is set to 0.01 (<1%), while 0.05 (<5%) outage and a peak data rate of 144 kbps [53] is enforced for the secondary network. Monte Carlo analysis on this model compares the analytical expression for outage with simulated results for various cases.

A. Feasibility of deployment

The feasible coverage radius of the secondary network as the distance between the DTV transmitter and the secondary BS increases is explored first to evaluate the scale of coexistence opportunity. To this end, an idealized scenario of the absence of shadowing and the case of perfect knowledge of the channel conditions are considered in figure 2a. It is observed that even with exact information on all the active DTV receivers, the maximum link distances for uplink communication in the secondary network fall off rapidly as the distance from the DTV transmitter $\text{Tx}^{(D)}$ increases. As the distance from $\text{Tx}^{(D)}$ increases, the margin of excess SNR available at any DTV receiver decreases due to increased path loss. Correspondingly, the maximum transmit power that can be used by the Secondary transmitter $\text{Tx}^{(S)}$ while maintaining the desired outage conditions reduces. The presence of shadowing with a large shadowing coefficient (9.6 dB) [54], [55] almost halves the allowed radius. However, if the OTA TV ownership rate of 60%, as well as the peak channel ratings at 70%, are factored in, there is a significant improvement in the link coverage as shown in figure 2b. Interestingly, urban clusters offer very small coverage radiuses when OTA TV ownership rates are not taken into account. However, since the OTA TV ownership rate is significantly low due to access to other means of TV access, the secondary coverages improve significantly. Conversely, in the rural areas where the households are spaced wide apart, the increased OTA TV ownership rate [56] limits the scope of coverage radius expansion. Thus, such a deployment can be used for low data rate applications in small coverage areas. Figure 2c highlights the bounds on the coverage distances that are possible using such a deployment. When highest data rate of 320 kbps is required, least coverage distances would be possible as the amount of interference caused by transmitting in all time slots on all subcarriers limits the maximum usable transmit power. Analogously, least data rates of 4.4 kbps provide the highest coverage distances.

With the feasibility and upper limits of such a deployment established, the impact of having varying degrees of information about the active DTV receivers is evaluated. First, the model selection for the Kriging method is explained. Then, link coverage and outage analysis results are presented for various cases considered.

B. Choice of semivariogram model and dependence on the number of sample points

Figure 4a shows a signal distribution on a 1 km^2 grid at 1 m resolution with the DTV transmitter located at the origin. A shadowing decorrelation distance of 30 m has been used to represent a typical urban scenario. Since an analytical semivariogram needs to be used for deducing the weights $\mathbf{w}$, Gaussian and Exponential semivariograms were evaluated with a bin size of 40 sample points and are shown in Figure 3a. Assuming that the deployment density of the secondary nodes is not going to be too sparse, the goodness of semivariogram fit at smaller lag distances is considered to be a good indicator of performance [51]. Further, the RMSE performance of the variograms is shown in Figure 3b. Since the path loss-based estimation method cannot estimate the shadowing coefficient, its RMSE is constant at the considered shadowing standard deviation σ_D. It is observed that the exponential semivariogram outperforms the Gaussian semivariogram when the number of samples is relatively small. The performance of both exponential and Gaussian semivariogram models is similar when the number of samples is large. Thus, the exponential semivariogram model is used for the rest of the analysis.

The accuracy of Ordinary Kriging is invariably better than the path loss-based method as it incorporates the effects of spatial correlation as well. Figure 4b shows the estimated signal plot using the exponential semivariogram with 400 sample points uniformly distributed across the grid with a minimum separation of 40 m. The number of secondary nodes is expected to be at least equal to the number of DTV receivers. Thus, for the remainder of this section, it is assumed that secondary nodes are also distributed with a similar deployment density as the DTV receiver nodes. However, it must be noted that the performance of Ordinary Kriging interpolation for a given number of sample points depends on various environmental factors such as decorrelation distance. The presence of a strong underlying spatial trend can lead to degraded performance, as the assumption of a constant mean may not hold. This is particularly relevant in areas very close to the DTV transmitter, where the distance from the DTV transmitter is a stronger determinant for signal deviations than the shadowing component [34]. Under such circumstances,

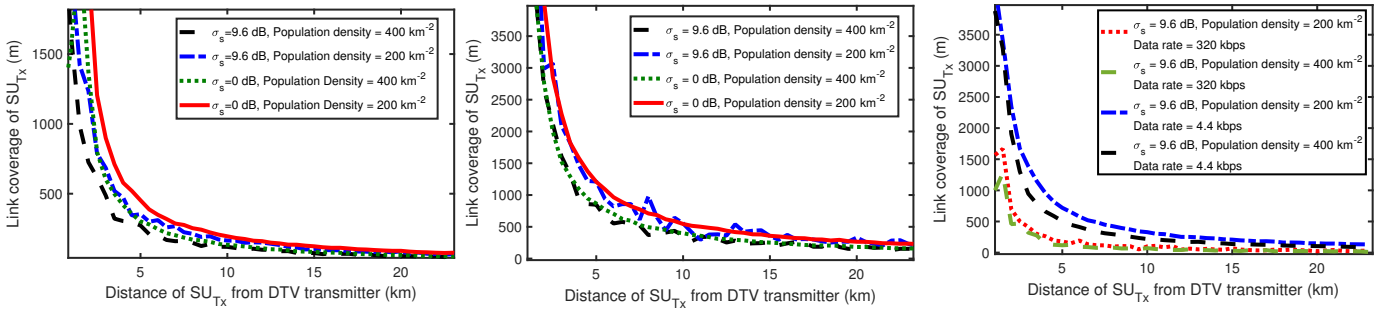

Fig. 2. Comparison of maximum secondary link distances under idealized conditions with and without shadowing, and complete CSI information (a) Without factoring in viewership statistics (b) After factoring in OTA TV ownership and peak viewership statistics p_{act} = 0.7. $p^{(D)}_{out,th}$ = 0.01, $p^{(S)}_{out,th}$ = 0.05, Minimum data rate = 4.4 kbps. (c) Upper and lower bounds on secondary link distances under idealized conditions after factoring in OTA TV ownership and peak viewership statistics p_{act} = 0.7. $p^{(D)}_{out,th}$ = 0.01, $p^{(S)}_{out,th}$ = 0.05.

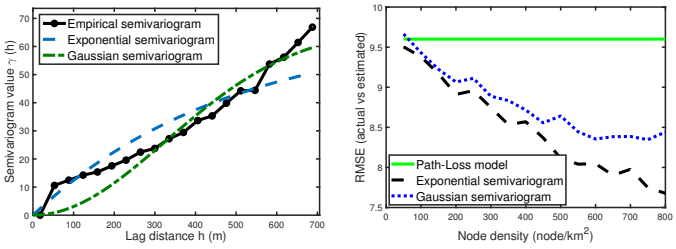

Fig. 3. (a) Empirical and estimated semivariograms. Number of sampling points (N) = 400; minimum sample separation = 40 m. (b) RMSE performance of exponential and Gaussian variograms with varying number of sampling points. Shadowing coefficient (σ_D) = 9.6 dB, shadowing decorrelation distance = 30 m.

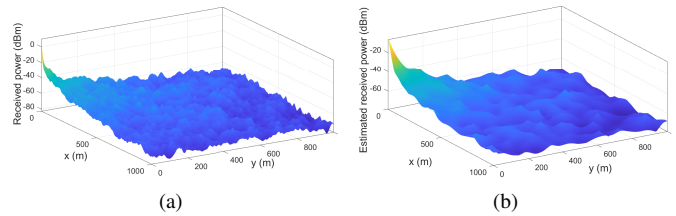

Fig. 4. (a) Actual signal map for a 1 km^2 grid with DTV tower at (0, 0), resolution 1 m; (b) Estimated signal map using exponential semivariogram with 400 sample points uniformly distributed in the region.

a combination of local trend fitting and Ordinary Kriging is suggested.

C. Performance of the secondary network

The coverage radius and outage performance of the secondary deployment using Kriging was evaluated for typical rural and urban settings. In line with the observations made with the ideal coverage curves in Fig. 2, the coverage plots in Fig. 5 indicate decreasing coverage radiuses as the distance of the BS Rx$^{(S)}$ increases from the DTV transmitter Tx$^{(D)}$. It is observed that when Kriging interpolation is used with the notion of a hypothetical critical DTV receiver at an estimated separation of d_c from Tx$^{(S)}$, the coverage radius is more conservative as compared to that estimated by the statistical path loss model. However, it is observed in Fig. 5c that the outage performance when using the Kriging method is well within the required outage constraints of $p^{(D)}_{out} \leq 0.01$. This is due to increased accuracy of the signal map, which produces tighter bounds. However, when exact DTV receiver locations are known to the secondary network, the coverage radius approaches the ideal values while the path loss model doesn't offer much improvement as the path loss model discards any other information other than that of the critical DTV receiver. Thus, the use of Kriging interpolation greatly enhances the prospects of viable secondary network deployment in the TVBS as compared to a simple path loss model-based estimation.

D. Geospatial maps and viewership statistics

Fig. 6 shows the combined use of geospatial mapping and the Kriging technique. Fig. 6a is a 25km $\times$ 25km demographic map of a metropolitan area and its adjoining urban-cluster with the household locations tagged. The DTV Tower is located at the lower left corner (origin) and the population density is approximately 1000 households per square kilometers, typical of metropolitan cities. Jakes model is used to generate the path loss and shadowing map in the entire region, and a sample of points is taken for Kriging estimation. The variation of average coverage radius of the secondary networks with distance from the DTV tower for a minimum data rate of 4.4 kbps is shown in Fig. 6b. Here, the OTA TV ownership of 70% [57]is considered with prime-time channel ratings (and hence the probability of DTV receiver being active) taken as 60%. Fig. 6c shows how the coverage radius varies across multiple viewership conditions typically observed through various parts of the day when Kriging-based estimation is used, and the locations of active DTV receivers are estimated using geospatial maps.

The observations from Fig. 6b are congruent with the earlier remarks. The coverage radius shrinks where the density of active DTV receivers is high and expands substantially in areas of sparse DTV viewership such as the area around the 10 km radius from the DTV tower. However, a consistent path loss statistical model is not able to incorporate this change in

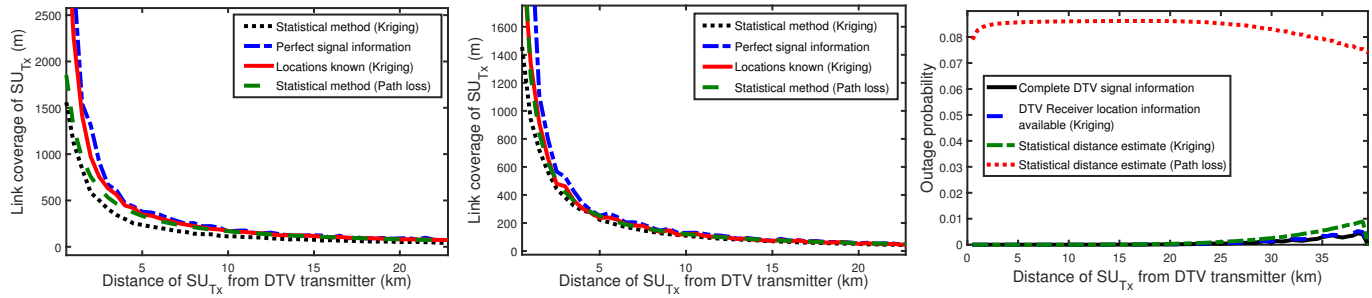

(a) (b) (c)

Fig. 5. Variation of secondary coverage range at minimum supported data rate (4.4 kbps) as the distance of secondary BS increases from the DTV transmitter for, (a)Rural areas, population density ($\lambda = 200\text{km}^{-2}$) (b)Urban clusters, population density ($\lambda = 400\text{km}^{-2}$); (c) Variation of DTV receiver outages at minimum supported data rate (4.4 kbps) as the distance of secondary BS increases from the DTV transmitter for urban clusters, population density ($\lambda = 400\text{km}^{-2}$); $p_{out,th}^{(D)}$ = 0.01, $p_{out,th}^{(S)}$ = 0.05.

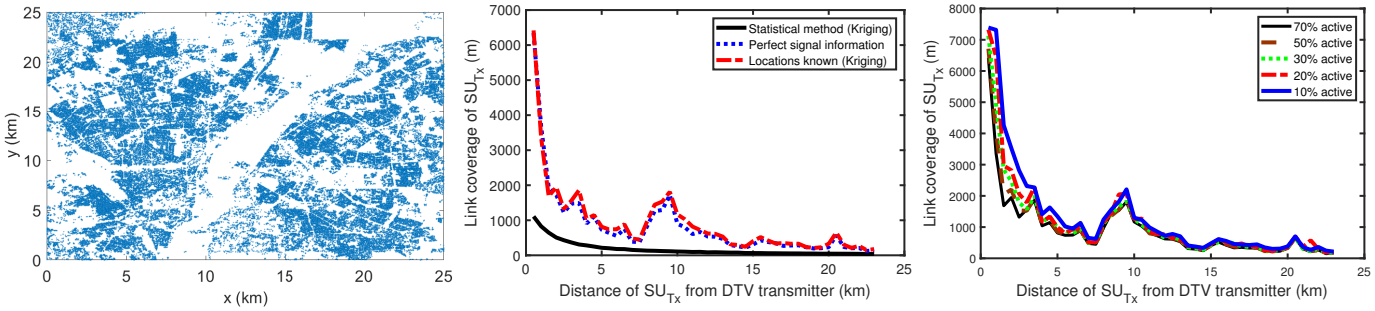

(a) (b) (c)

Fig. 6. (a) Map of buildings in a metro city and adjoining areas. (b) Secondary uplink coverage range computed for the given buildings map with Kriging interpolation with 70% active users. (c) Secondary uplink coverage range computed for the given buildings map for different fractions of active users; $p_{out,th}^{(D)}$ = 0.01, $p_{out,th}^{(S)}$ = 0.05.

population dynamics in the model. Fig. 6c shows the fluctuation of coverage radius of secondary nodes with the changing dynamics of DTV viewership. It indicates that the leeway afforded by incorporating the changing viewership dynamics has a marginal impact on the coverage radius beyond what has been achieved by the use of the Kriging method as a whole. Further, it must be considered that the values of environmental factors such as the shadowing coefficient, shadowing correlation, and path loss factor used in the simulations have a huge dependence on the environment when considering an actual deployment. For example, a lower shadowing coefficient can improve the range of distances in the secondary network as the margin of error reduces. Further, local shadowing trends are typically observed in empirical studies [34] where the values of these parameters may change within geographical pockets [54]. Kriging interpolation is well suited to estimate the signal conditions under such conditions as compared to statistical models.

VI. Concluding Remarks

The scenario of deploying low data rate secondary networks in co-channel mode inside the DTV coverage area has been explored in this study. As observed from this study, having a granular mapping of DTV receiver locations significantly improves the secondary network performance without compromising the performance of the DTV broadcast network even when signal estimation techniques such as Kriging are used. In DTV networks, this may be enabled by leveraging the provisions of an in-band dedicated return channel in various standards like DVB-RCT and ATSC 3.0 and making this information available to the secondary network. The mechanism through which more reliable information may be made available to the secondary network will be taken up in future studies.

The use of channel viewership statistics shows a limited upside potential of having frequent feedback as the viewership statistics fluctuate throughout the day. Availability of DTV receiver information enables the secondary base stations to dynamically adapt to the arrival or departure of DTV receivers in their coverage regions (when DTV receivers are tuned to or away from the current DTV band), and hence improve network performance and interference management. Further, rooftop antennas are usually employed for static DTV receivers, while the secondary nodes may be present on the ground. It has been noted in [58] that there is a huge disparity in the signal conditions on the rooftops and the ground due to the height of buildings and the occlusion created by the surrounding buildings. Thus, the accuracy of spatially mapped REMs can be further improved by considering the three-dimensional aspects of signal propagation as well, which is expected to

further increase the performance of the secondary network.

APPENDIX A
CO-CHANNEL INTERFERENCE AT DTV RECEIVER

Let $r^{(D)}(t)$ be the OFDM signal received by the DTV receiver $\text{Rx}^{(D)}$ from the DTV transmitter $\text{Tx}^{(D)}$. $r^{(D)}(t)$ is expressed as

$$r^{(D)}(t) = \frac{1}{\sqrt{T_u^{(D)}}} \sum_{l' \in \mathbb{Z}} \sum_{k'=0}^{N^{(D)}-1} h^{(D)} X_{k'}^{(D)}[l'] e^{j2\pi \frac{k'(t-\tau_n^{(D)})}{T_u^{(D)}}} \times \prod \left(\frac{t - l'T^{(D)} + T_g^{(D)} - \tau_n^{(D)}}{T^{(D)}} \right) \quad \text{(A.1)}$$

where $N^{(D)}$ is the number of active subcarriers in the DTV network, $X_{k'}^{(D)}$ is the data symbol transmitted in the l'th block on the k'th subcarrier, $T_u^{(D)}$ and $T_g^{(D)}$ are respectively the useful symbol period and guard interval, with $T^{(D)} = T_u^{(D)} + T_g^{(D)}$. $\tau_n^{(D)}$ and $h^{(D)}$ are respectively the delay introduced and impulse response of the received signal. Similarly, for the secondary transmission, the interference signal received at the DTV receiver $\text{Rx}^{(D)}$ from the secondary transmitter $\text{Tx}^{(S)}$ is $r^{(S)}(t)$ would be

$$r^{(S)}(t) = \frac{e^{j2\pi\Delta f^{(S)}t}}{\sqrt{T_u^{(S)}}} \left(\sum_{l \in \mathbb{Z}} \sum_{k=0}^{N^{(S)}-1} h^{(S)} X_k^{(S)}[l] e^{j2\pi \frac{k'(t-\tau^{(S)}+t_{\text{off}})}{T_u^{(S)}}} \times \prod \left(\frac{t - lT^{(S)} + T_g^{(S)} - \tau^{(S)} + t_{\text{off}}}{T^{(S)}} \right) \right). \quad \text{(A.2)}$$

Here, $\tau^{(S)}$, and $h^{(S)}$ are respectively the delay introduced, and impulse response for the secondary signal. $X_k^{(S)}$ is the data symbol transmitted in lth OFDM block of the secondary signal on the kth subcarrier during the period $T_u^{(D)}$. $\Delta f^{(S)}$ is the frequency offset between the DTV and secondary signals. t_{off} is a uniformly distributed random delay offset in $(0, T_u^{(D)})$ introduced due to lack of synchronization of symbol start boundaries of the DTV and secondary OFDM symbols at the DTV receiver. Considering each secondary symbol duration as a time slot, let ξ' be the number of time slots a secondary signal is transmitted within one DTV broadcast symbol duration. With $T_u^{(D)} \gg T_u^{(S)}$, ξ' can take a value in $(0, \xi'_{\max})$, where $\xi'_{\max} = \left\lceil \frac{T_u^{(D)}}{T^{(S)}} \right\rceil$. Interference caused by the secondary signal at DTV receiver varies as a function of the number of active subcarriers $N^{(S)}$ and the number of occupied time slots ξ'. The DTV receiver processes both signals using the same basis functions. The OFDM decomposition basis function for a DVB symbol's p'th subcarrier is expressed as

$$\Phi_{p'}^{(D)} = \frac{1}{\sqrt{T_u^{(D)}}} e^{-j2\pi \frac{p't}{T_u^{(D)}}} \prod \left(\frac{t}{T_u^{(D)}} \right). \quad \text{(A.3)}$$

For the DTV signal, the desired OFDM symbol at the p'th subcarrier is expressed as

$$\tilde{X}_{p'}^{(D)} = X_{p'}^{(D)} H_{p'}^{(D)}$$

where $\tilde{X}_{p'}^{(D)} = \int_{\mathbb{R}} r^{(D)}(t) \Phi_{p'}^{(D)}(t) dt$ and $H_{p'}^{(D)} = h_{p'}^{(D)} e^{-j2\pi \frac{p'\tau^{(D)}}{T_u^{(D)}}}$. For the interference signal $I_{p'}$ at the p'th subcarrier,

$$I_{p'} = \int_{\mathbb{R}} r^{(S)}(t) \Phi_{p'}^{(D)}(t) dt. \quad \text{(A.4)}$$

The basis function (A.3) decomposes the received DTV signal (A.1) as well as the secondary signal (A.2) over the p'th DTV subcarrier of the DTV transmission. The secondary signal is unwanted at the DTV receiver as it causes interference in reception. The interfering signal after decomposition using (A.3) can be expressed as

$$\begin{aligned} I_{p'} &= \int_{\mathbb{R}} r^{(S)}(t) \Phi_{p'}^{(D)}(t) dt \\ &= \frac{1}{\sqrt{T_u^{(D)} T_u^{(S)}}} \left(\int_{\mathbb{R}} \sum_{l \in \mathbb{Z}} \sum_{n=1}^{L} h_n^{(S)} \sum_{k=0}^{N^{(S)}-1} X_k^{(S)}[l] \right. \\ &\quad e^{j2\pi c(k)t} e^{-j2\pi \frac{k\tau^{(S)}}{T_u^{(S)}}} e^{-j2\pi \frac{kt_{\text{off}}}{T_u^{(S)}}} \prod \left(\frac{t}{T_u^{(D)}} \right) \\ &\quad \left. \prod \left(\frac{t - lT^{(S)} - \tau^{(S)} + T_g^{(S)} + t_{\text{off}}}{T^{(S)}} \right) dt \right) \end{aligned} \quad \text{(A.5)}$$

where $c(k) = \Delta f^{(S)} + \frac{k}{T_u^{(S)}} - \frac{p'}{T_u^{(D)}}$. The effective integration period in (A.5) depends on the normalized windowing functions $\prod(\cdot)$ for the DTV receiver's basis function and the secondary signal, which are expressed as

$$\prod \left(\frac{t}{T_u^{(D)}} \right) = 1 \text{ iff } 0 \le t \le T_u^{(D)}$$

$$\prod \left(\frac{t - lT^{(S)} - \tau^{(S)} + T_g^{(S)} + t_{\text{off}}}{T^{(S)}} \right) = 1 \text{ iff } lT^{(S)} + T_r \le t \le (l+1)T^{(S)} + T_r$$

where $T_r = \tau^{(S)} - t_{\text{off}} - T_g^{(S)}$. If ξ' secondary symbols are received in a DTV symbol's useful duration $T_u^{(D)}$, (A.5) can be expressed as the sum of interference due to each secondary signal.

Applying the integration limits to (A.5) and solving yields (A.6), where $c(k) = \Delta f^{(S)} + \frac{k}{T_u^{(S)}} - \frac{p'}{T_u^{(D)}}$. The average interference power at the p'th subcarrier for a given t_{off} can then be expressed as (A.7), where $\omega \triangleq \tau^{(S)} - t_{\text{off}} - T_g^{(S)}$. Averaging (A.7) over t_{off}, we have

$$\mathbb{E}\left[\mid I_{p'}^{(S)}[m] \mid^2 \right] = \int_0^{T^{(S)}} \mathbb{E}[\mid I_{p'}^{(S)}[m] \mid^2]_{t_{\text{off}}} dt_{\text{off}}. \quad \text{(A.8)}$$

Solving (A.8) yields the result in (16). The reader is directed

$$I_{p'} = \frac{1}{\sqrt{T_u^{(D)} T_u^{(S)}}} \left[\sum_{k=0}^{N^{(S)}-1} H_k^{(S)} e^{j2\pi \frac{kt_{\text{off}}}{T_u^{(S)}}} \left(X_k^{(S)}[l] \frac{\sin(\pi c(k)((lT^{(S)} + \tau^{(S)} - t_{\text{off}} - T_g^{(S)}))}{\pi c(k)} \times e^{j\pi c(k)(lT^{(S)} + \tau^{(S)} - t_{\text{off}} - T_g^{(S)})} \right.\right.$$
$$+ \sum_{b=1}^{\lfloor \xi' \rfloor - 1} X_k^{(S)}[l+b] \frac{\sin(\pi c(k) T^{(S)})}{\pi c(k)} \times e^{j\pi c(k)((2l+2b-1)T^{(S)} + 2\tau^{(S)} - 2t_{\text{off}} - 2T_g^{(S)})} \tag{A.6}$$
$$\left.\left. + \; X_k[l + \lfloor \xi' \rfloor] \frac{\sin(\pi c(k)(\xi' T^{(S)} - (l + \lfloor \xi' \rfloor) T^{(S)} - \tau^{(S)} + t_{\text{off}} + T_g^{(S)}))}{\pi c(k)} \times e^{j\pi c(k)(\xi' T^{(S)} + (l + \lfloor \xi' \rfloor) T^{(S)} + \tau^{(S)} - t_{\text{off}} - T_g^{(S)})} \right) \right].$$

$$\mathbb{E}\left[\mid I_{p'}^{(S)}[m] \mid^2 \right]_{t_{\text{off}}} = \frac{1}{T_u^{(S)} T_u^{(D)}} \sum_{k=0}^{N^{(S)}-1} \mid H_k^{(S)} \mid^2 \left\{ \frac{\sin^2(\pi c(k)(T^{(S)} + \omega))}{\pi^2 c^2(k)} + \sum_{b=0}^{\lfloor \xi' \rfloor - 1} \frac{\sin^2(\pi c(k) T^{(S)})}{\pi^2 c^2(k)} + \frac{\sin^2(\pi c(k)((\xi' - \lfloor \xi' \rfloor) T^{(S)} - \omega))}{\pi^2 c^2(k)} \right\}. \tag{A.7}$$

to [13] for a comprehensive proof.

REFERENCES

[1] H. Bezabih, B. Ellingsaeter, J. Noll, and T. T. Maseng, "Digital broadcasting: Increasing the available white space spectrum using TV receiver information," *IEEE Veh. Technol. Mag.*, vol. 7, no. 1, pp. 24–30, 2012.

[2] P. Palka and P. Neumann, "Analyzing the availability of TV white spaces in dynamic broadcast," *IEEE Trans. Consum. Electron.*, vol. 60, no. 3, pp. 302–310, 2014.

[3] Z. Zhao, M. C. Vuran, D. Batur, and E. Ekici, "Shades of white: Impacts of population dynamics and TV viewership on available TV spectrum," *IEEE Trans. Veh. Technol.*, vol. 68, no. 3, pp. 2427–2442, 2019.

[4] N. Co., "The nielsen local watch report: The evolving over-the-air home," Nielsen Co., "New York, NY, USA", Tech. Rep., Apr. 2019. [Online]. Available: https://www.nielsen.com/wp-content/uploads/sites/3/2019/04/q2-2018-local-watch-report.pdf

[5] R. Martinez Alonso, D. Plets, M. Deruyck, L. Martens, G. Guillen Nieto, and W. Joseph, "TV white space and LTE network optimization toward energy efficiency in suburban and rural scenarios," *IEEE Trans. Broadcast.*, vol. 64, no. 1, pp. 164–171, 2018.

[6] J. van de Beek, J. Riihijarvi, A. Achtzehn, and P. Mahonen, "TV white space in Europe," *IEEE Trans. Mobile Comput.*, vol. 11, no. 2, pp. 178–188, 2012.

[7] P. J. Smith, P. A. Dmochowski, H. A. Suraweera, and M. Shafi, "The effects of limited channel knowledge on cognitive radio system capacity," *IEEE Trans. Veh. Technol.*, vol. 62, no. 2, pp. 927–933, 2013.

[8] K. Sato and T. Fujii, "Kriging-based interference power constraint: Integrated design of the radio environment map and transmission power," *IEEE Trans. Cogn. Commun. Netw.*, vol. 3, no. 1, pp. 13–25, 2017.

[9] G. Martínez-Pinzón, N. Cardona, C. Garcia-Pardo, A. Fornés-Leal, and J. A. Ribadeneira-Ramírez, "Spectrum sharing for LTE-A and DTT: Field trials of an indoor LTE-A femtocell in DVB-T2 service area," *IEEE Trans. Broadcast.*, vol. 62, no. 3, pp. 552–561, Sep. 2016.

[10] L. Bedogni, A. Achtzehn, M. Petrova, P. Mähönen, and L. Bononi, "Performance assessment and feasibility analysis of IEEE 802.15.4m wireless sensor networks in TV grayspaces," *ACM Trans. Sen. Netw.*, vol. 13, no. 1, Jan. 2017.

[11] V. Popescu, M. Fadda, M. Murroni, J. Morgade, and P. Angueira, "Co-channel and adjacent channel interference and protection issues for DVB-T2 and IEEE 802.22 WRAN operation," *IEEE Trans. Broadcast.*, vol. 60, no. 4, pp. 693–700, Dec. 2014.

[12] J. Sachs, I. Maric, and A. Goldsmith, "Cognitive cellular systems within the TV spectrum," in *Proc. IEEE Symp. New Frontiers in Dynamic Spectrum (DySPAN)*, 2010, pp. 1–12.

[13] A. Thakur, S. De, and G. M. Muntean, "Co-channel secondary deployment over DTV bands using reconfigurable radios," *IEEE Trans. Veh. Technol.*, vol. 69, no. 10, pp. 12 202–12 215, 2020.

[14] A. Thakur, S. De, and G. Muntean, "Interference-aware co-channel transmission over DTV bands via partial frequency and time overlaps," in *Proc. Intl. Conf. Commum. (ICC)*, May 2019, pp. 1–6.

[15] Y. Selén, R. Baldemair, and J. Sachs, "A short feasibility study of a cognitive TV black space system," in *Proc. IEEE Intl. Symp. Personal, Indoor and Mobile Radio Communications*, 2011, pp. 520–524.

[16] K. Woyach, P. Grover, and A. Sahai, "Near vs. far field: Interference aggregation in TV whitespaces," in *Proc. IEEE GLOBECOM*, 2011, pp. 1–5.

[17] C. Lee and M. Haenggi, "Interference and outage in poisson cognitive networks," *IEEE Trans. Wireless Commun.*, vol. 11, no. 4, pp. 1392–1401, 2012.

[18] B. Gao, S. Bhattarai, J. J. Park, Y. Yang, M. Liu, K. Zeng, and Y. Dou, "Incentivizing spectrum sensing in database-driven dynamic spectrum sharing," in *Proc. IEEE Intl. Conf. Comput. Commun.*, 2016, pp. 1–9.

[19] D. Xue, E. Ekici, and M. C. Vuran, "Cooperative spectrum sensing in cognitive radio networks using multidimensional correlations," *IEEE Trans. Wireless Commun.*, vol. 13, no. 4, pp. 1832–1843, 2014.

[20] Z. Shi, W. Gao, S. Zhang, J. Liu, and N. Kato, "Machine learning-enabled cooperative spectrum sensing for non-orthogonal multiple access," *IEEE Tran. Wireless Commun.*, vol. 19, no. 9, pp. 5692–5702, 2020.

[21] S. Agarwal and S. De, "Rural broadband access via clustered collaborative communication," *IEEE/ACM Trans. Netw.*, vol. 26, no. 5, pp. 2160–2173, Oct. 2018.

[22] D. Plets, Wout Joseph, E. Tanghe, Leen Verloock, and Luc Martens, "Analysis of propagation of actual DVB-H signal in a suburban environment," in *Proc. IEEE Antennas and Propagation Soc. Intl. Symp.*, 2007, pp. 1997–2000.

[23] P. Bagot, M. Beach, A. Nix, J. McGeehan, and J. Boyer, "Spatially adaptive TV broadcast system: Hardware in the loop operational analysis," *IEEE Trans. Broadcast.*, vol. 64, no. 1, pp. 41–51, 2018.

[24] P. Angueira, M. Velez, D. De La Vega, A. Arrinda, and J. L. Ordiales, "Fading caused by moving vehicles near the receiver on DTV (COFDM) 8-MHz signals," *IEEE Commun. Lett.*, vol. 6, no. 6, pp. 250–252, 2002.

[25] S. Yin, D. Chen, Q. Zhang, M. Liu, and S. Li, "Mining spectrum usage data: A large-scale spectrum measurement study," *IEEE Trans. Mobile Comput.*, vol. 11, no. 6, pp. 1033–1046, 2012.

[26] X. Ying, J. Zhang, L. Yan, Y. Chen, G. Zhang, M. Chen, and R. Chandra, "Exploring indoor white spaces in metropolises," *ACM Trans. Intell. Syst. Technol.*, vol. 9, no. 1, Aug. 2017.

[27] X. Zhang and E. W. Knightly, "WATCH: WiFi in active TV channels," *IEEE Trans. Cogn. Commun. Netw.*, vol. 2, no. 4, pp. 330–342, 2016.

[28] S. Huang, X. Liu, and Z. Ding, "Decentralized cognitive radio control based on inference from primary link control information," *IEEE J. Sel. Areas Commun.*, vol. 29, no. 2, pp. 394–406, 2011.

[29] B. Wild and K. Ramchandran, "Detecting primary receivers for cognitive radio applications," in *Proc. IEEE Symp. New Frontiers in Dynamic Spectrum Access Networks (DySPAN)*, Nov 2005, pp. 124–130.

[30] S. Mishra, "Maximizing available spectrum for cognitive radios," Dept. Comput. Sci. Eng., Univ. California Berkeley, Berkeley, Ph.D. dissertation, Jan. 2010.

[31] ATSC, "ATSC proposed standard: Dedicated return channel for ATSC 3.0," Advanced Television Systems Committee (ATSC), Standard A/323, 12 2018. [Online].

Available: https://www.atsc.org/wp-content/uploads/2017/11/A323S32-293r21-Dedicated-Return-Channel.pdf
[32] K. Harrison and A. Sahai, "Seeing the bigger picture: Context-aware regulations," in *IEEE Intl. Symp. on Dynamic Spectrum Access Networks*, 2012, pp. 21–32.
[33] Ofcom, "Implementing TV white spaces," The Office of Communications (Ofcom), Technical Report (TR), 02 2015.
[34] A. Achtzehn, J. Riihijärvi, and P. Mähönen, "Improving accuracy for TVWS geolocation databases: Results from measurement-driven estimation approaches," in *IEEE DYSPAN*, 2014, pp. 392–403.
[35] Z. Han, J. Liao, Q. Qi, H. Sun, and J. Wang, "Radio Environment Map Construction by Kriging Algorithm Based on Mobile Crowd Sensing," *Wirel. Commun. Mob. Com.*, vol. 2019, p. 12, 2019.
[36] J. Perez-Romero, A. Zalonis, L. Boukhatem, A. Kliks, K. Koutlia, N. Dimitriou, and R. Kurda, "On the use of radio environment maps for interference management in heterogeneous networks," *IEEE Commun. Mag.*, vol. 53, no. 8, pp. 184–191, 2015.
[37] S. Capkun, M. Hamdi, and J. . Hubaux, "Gps-free positioning in mobile ad-hoc networks," in *Proc. Annual Hawaii Intl. Conf. System Sciences*, Jan. 2001.
[38] Y. Kim, B. Lee, H. So, D.-H. Hwang, and S.-C. Kim, "Cooperative localization considering estimated location uncertainty in distributed ad hoc networks," *Int. J. Distrib. Sens. N.*, vol. 14, no. 2, p. 1550147718759634, 2018.
[39] B. Zhou, Q. Chen, H. Wymeersch, P. Xiao, and L. Zhao, "Variational inference-based positioning with nondeterministic measurement accuracies and reference location errors," *IEEE Trans. Mobile Comput.*, vol. 16, no. 10, pp. 2955–2969, Oct. 2017.
[40] A. Sobehy, E. Renault, and P. Muhlethaler, "Position certainty propagation: A localization service for ad-hoc networks," *Computers*, vol. 8, no. 1, 2019.
[41] D. Denkovski, V. Atanasovski, L. Gavrilovska, J. Riihijärvi, and P. Mähönen, "Reliability of a radio environment map: Case of spatial interpolation techniques," in *2012 ICST Conference on Cognitive Radio Oriented Wireless Networks and Communications (CROWNCOM)*, 2012, pp. 248–253.
[42] S. Bi, J. Lyu, Z. Ding, and R. Zhang, "Engineering Radio Maps for Wireless Resource Management," *IEEE Wireless Commun.*, vol. 26, no. 2, pp. 133–141, Apr. 2019.
[43] G. Boccolini, G. Hernández-Peñaloza, and B. Beferull-Lozano, "Wireless sensor network for spectrum cartography based on Kriging interpolation," in *Proc. IEEE PIMRC*, 2012, pp. 1565–1570.
[44] K. Tsukamoto, M. Kitsunezuka, and K. Kunihiro, "Highly accurate radio environment mapping method based on transmitter localization and spatial interpolation in urban los/nlos scenario," in *Proc. IEEE WiSNet*, 2018, pp. 5–7.
[45] S. J. Salamon, H. J. Hansen, and D. Abbott, "Universal kriging prediction of line-of-sight microwave fading," *IEEE Access*, vol. 8, pp. 74 743–74 758, 2020.
[46] H. Xia, S. Zha, J. Huang, and J. Liu, "Radio environment map construction by adaptive ordinary kriging algorithm based on affinity propagation clustering," *International Journal of Distributed Sensor Networks*, vol. 16, no. 5, p. 1550147720922484, 2020.
[47] K. Sato, K. Inage, and T. Fujii, "On the performance of neural network residual kriging in radio environment mapping," *IEEE Access*, vol. 7, pp. 94 557–94 568, 2019.
[48] D. Mao, W. Shao, Z. Qian, H. Xue, X. Lu, and H. Wu, "Constructing accurate radio environment maps with kriging interpolation in cognitive radio networks," in *2018 Cross Strait Quad-Regional Radio Science and Wireless Technology Conference (CSQRWC)*, 2018, pp. 1–3.
[49] K. Sato, K. Inage, and T. Fujii, "Modeling the Kriging-aided spatial spectrum sharing over log-normal channels," *IEEE Wireless Commun. Lett.*, vol. 8, no. 3, pp. 749–752, 2019.
[50] Z. Zhao, M. C. Vuran, D. Batur, and E. Ekici, "Ratings for spectrum: Impacts of TV viewership on TV whitespace," in *Proc. IEEE GLOBECOM*, 2014, pp. 941–947.
[51] N. A. C. Cressie, *Statistics for Spatial Data*. Wiley, 1993.
[52] H. Ritchie and M. Roser, "Urbanization," *Our World in Data*, 2018, https://ourworldindata.org/urbanization.
[53] S. Tabbane, "Session 5: NB-IoT networks," Traffic engineering and advanced wireless network planning, ITU Asia-Pacific Centre of Excellence Training, Monterey, CA, Oct. 2018.
[54] K. Sato, K. Inage, and T. Fujii, "Frequency correlation of shadowing over tv bands in suburban area," *Electronics Letters*, vol. 54, pp. 6–8(2), January 2018.
[55] T. Schwengler, "Wireless and Cellular Communications Class Notes for tlen-5510," Lecture Notes, 2019.
[56] N. A. of Broadcasters, "Broadcast television and radio in rural communities," National Association of Broadcasters, Washington, DC, USA, Tech. Rep., May 2018. [Online]. Available: https://www.nab.org/broadcastIssues/rural.pdf
[57] BARC, "Tv universe estimates 2020," Broadcast Audience Research Council India (BARC), Technical Report (TR), 2018. [Online]. Available: https://www.barcindia.co.in/whitepaper/barc-india-tv-universe-estimates-2020.pdf
[58] L. Bedogni, A. Trotta, and M. Di Felice, "On 3-dimensional spectrum sharing for TV white and gray space networks," in *Proc. IEEE WoWMoM*, 2015, pp. 1–8.